# Fronts and Convective Cold Pools in the Oklahoma Mesonet. Part II: Case Studies

Andrew T. Lesage[*] and Steven K. Krueger

*Department of Atmospheric Sciences, University of Utah, Salt Lake City, Utah*

[*]*Corresponding author address:* Andrew T. Lesage, Department of Atmospheric Sciences, 135 S

1460 E, Rm 819, Salt Lake City, Utah 84112-0110.

E-mail: andy.lesage@utah.edu

1

# ABSTRACT

Over 15 years of Oklahoma Mesonet observations thousands of frontal passages were detecting using Mesonet station temperature and pressure data. Cold pools were then identified using front and divergence requirements. These events were able to be further investigated in case studies. Four of these are detailed here: 1) 13 June 1997, 2) 15-16 June 2002, 3) 20 May 2011, and 4) 24-25 May 2011. Cold pool areas for the 4 cases are shown, as well as the location of the front as it passes through the Mesonet. Cold pools were similar in length to other studies; however, they generally only extended around 50-100 km behind the front. Cold pool duration was primarily 30-60 mins under the algorithm used. Divergence, temperature, and pressure time series highlight consistent patterns. Identifying front and cold pool characteristics could potentially be used in improving cold pool parameterizations.

## 1. Introduction

Convective downdrafts and cold pools have been a subject of investigation for over half a century. Fujita had identified three main surface pressure features in squall lines: the pressure surge line, the thunderstorm high, and the wake depression (Fujita 1955). The thunderstorm high was frequently co-located with a cold pool in convective systems. Downdrafts have been found to cause damage through strong surface outflow winds (Fujita and Wakimoto 1980; Coleman and Knupp 2011). Doppler radar and rawinsonde data have been used to analyze life cycles of thunderstorm outflow boundaries, also known as gust fronts (Wakimoto 1982). Wakimoto found that gust front edges were frequently the location of updrafts. High surface winds in the outflows are commonly found with slow propagation speeds, large amplitude pressure disturbances, and ambient winds of the same sign, such as a headwind with a pressure trough (Coleman and Knupp 2009)

Squall system analysis from a 1968 field campaign centered in Barbados detailed both convective saturated downdrafts and mesoscale unsaturated downdrafts at the 785 mb flight level in convective and rear regions of the squalls (Zipser 1977). In the Global Atmospheric Research Program Atlantic Tropical Experiment (GATE) ship data, the temperature depressions recovered faster than did water vapor. Cold pool wakes have been shown to recover faster if the downdraft region contains weaker subsidence (Johnson and Nicholls 1982). They found in GATE that the sensible heat flux increased an order of magnitude and the latent heat flux increased a factor of three in convective wakes.

Similar recovery results occurred in trade wind shallow cumulus cold pools during the Rain in Cumulus over the Ocean (RICO) experiment (Zuidema et al. 2012). Entrainment of drier air from above was suggested as the cause of specific humidities remaining constant after the initial recovery. They also found that mesoscale arcs occurred more frequently in areas of higher water

vapor paths. Gust fronts detected by radar in West Africa convection during the African Monsoon Multidisciplinary Analysis (AMMA) field campaign preferentially generated new deep convective cells in the area in which the density current passed (Dione et al. 2014).

Modeling studies have looked at downdraft and cold pool influences on convection. Colliding outflow boundaries have been modeled in 3-D numerical cloud models (Droegemeier and Wilhelmson 1985). It was found that collision areas were warmer and moister resulting in greater lifting of air over the cold pool aiding in the formation of new convection. Simulations of squall lines have shown that low-level shear can aid in deeper lifting at cold pool outflow boundaries allowing squall lines to maintain structure for several life cycles of convective cells (Rotunno et al. 1988).

Modeling of GATE ship array cases found that precipitation evaporation influences the wake height and thermodynamic characteristics (Nicholls and Johnson 1984). Without evaporative precipitation the mixed layer would be shallower with reduced surface fluxes due to a higher mixed layer temperature. Analysis of simulated trade wind cold pools from Rain In Cumulus over the Ocean (RICO) campaign data found updrafts close to the cold pool boundary were moister and had higher vertical velocity than updrafts further away from the cold pool (Li et al. 2014). They found that stronger near-surface winds led to higher surface fluxes.

Parameterizations have looked at convective cells for years; however, convective downdrafts were considered to be a lesser source of downward mass flux compared to the environment and thus were left out (Moorthi and Suarez 1991; Pan and Randall 1998). Neglecting the compensating cumulus downdraft mass fluxes tends to result in a too warm and dry lower troposphere (Johnson 1976). Later versions of models included downdrafts as well as exchanges between clouds and the environment (Cheng and Arakawa 1997; Kain and Fritsch 1990).

4

A step further has been in parameterizing cold pool processes. One attempt involved parameterizing cold pool area, depth, and propagation speed, treating the propagation like a gravity wave that recovers via surface and entrainment fluxes (Qian et al. 1998). The scheme performed reasonably well for GATE, Tropical Ocean and Global Atmosphere Coupled Ocean-Atmosphere Response Experiment (TOGA-COARE) cases and when incorporated in the NCAR Community Climate Model (CCM3), albeit with shallow, warm, and moist biases (Rozbicki et al. 1999).

Another method of parameterizing cold pools involved a prognostic variable, *org*, which attempted to capture the effects of convective organization on properties of entraining plumes (Mapes and Neale 2011). A higher *org* value resulted in more entrainment, precipitation, convective heating, and rain evaporation.

Cloud-system resolving simulations with parameterized large-scale circulation have found that convection remains disorganized with weak vertical shear, but larger vertical shear resulted in linear mesoscale systems (Anber et al. 2014). They found that high surface fluxes had higher organization even without shear, suggesting that, while shear can promote organization, it is not required. The more organized systems had more rain, larger mass fluxes, more cloud cover, higher vertical velocity, and higher moist static energy.

Increasing knowledge of cold pools in observational data is necessary to further improve representation of cold pools. This paper looks at cases from 15 yrs of Oklahoma Mesonet data. Section 2 details the methodology for analyzing frontal passages and cold pools. Section 3 covers results for four cases studies: 1) 13 June 1997, 2) 15-16 June 2002, 3) 20 May 2011, and 4) 24-25 May 2011. Section 4 summarizes the conclusions.

## 2. Methodology

The data used in this analysis comes from the Department of Energy Atmospheric Radiation Measurement (ARM) Program's Oklahoma Mesonet dataset (Brock et al. 1995; McPherson et al. 2007). The selected data covers over 100 non-panhandle stations at 5-minute frequency over the period 1997-2011 at roughly 40 km spacing.

The frontal passages were identified using the analysis method described in more detail in Part I (Lesage and Krueger 2016). Using 30-minute differences in diurnal and elevation adjusted temperature and pressure, calculated every 5 minutes, a unitless front score (FS) was calculated (Eq. 1).

$$\text{FS}(t) = -1 \text{ K}^{-1}(\Delta T)_{30} + 1 \text{ hPa}^{-1}(\Delta p)_{30}. \tag{1}$$

Fronts were defined to occur at Mesonet stations when the FS exceeded a minimum threshold of 3, while fronts were defined to occur at Mesonet triangles if the FS exceeded the minimum threshold at all three stations within a 2-hour span.

Cold pools were defined to occur at Mesonet triangles if the triangle experienced both a frontal passage and if the strong divergence threshold ($D_i > 10^{-4}\text{s}^{-1}$) was reached within half an hour before or an hour after the front reaches halfway across the triangle. The identified fronts and cold pools can be tracked across the Mesonet.

## 3. Case Study Results

Over the course of 15 yrs of Mesonet data, tens of thousands of frontal passages at triangles were detected in the Oklahoma Mesonet. Hundreds of events involving a front that sweeps through large portions of the Mesonet can be used for case studies. Four such cases will be shown in this section:

6

1) 13 June 1997, 2) 15-16 June 2002, 3) 20 May 2011, and 4) 24-25 May 2011. These cases are supplemented with radar images from the UCAR image archive.

*a. 13 June 1997 Case*

At approximately 0000 UTC on 13 June 1997 a squall line, which initiated in southeastern Colorado and northeastern New Mexico, entered Kansas, the Oklahoma panhandle, and Texas. The disorganized line of thunderstorms reached the Mesonet grid at roughly 0300 UTC and was tracked for the next seven hrs across the Mesonet (Fig. 1) with isolated thunderstorms popping up ahead of the main line. At 0330 UTC (Fig. 1a) the front analysis found only smaller segments of a front (yellow and magenta segments for fronts and strong fronts, respectively) in western and northwestern portions of Oklahoma. The radar images show a gap between two thunderstorms that coincides with the lack of strong convergence (the gap in the red dots in Fig. 1a). In the areas where a front was defined, convergence was present to the east ahead of the front and divergence to the west behind the front. At 0330 UTC there was only one triangle designated as in a cold pool, located in the northwestern corner of the Mesonet domain.

From the 0500 UTC front analysis (Fig. 1b), the stronger, more well-defined front marked the leading edge of the system which had been organizing over the previous two hours. There was some bowing of the front present with trailing stratiform precipitation. The squall line had caught up to the isolated thunderstorms that developed ahead of the line. The area ahead of the front had strong convergence while strong divergence was present behind the front. Farther behind the front, near the back edge of the stratiform precipitation, there was a second region of convergence where a one-triangle front is marked. The analysis was designed to capture the strongest fronts at each triangle and in this instance this latter front was stronger at that particular triangle than when the initial line passed through heading eastward. This was likely a result of the squall line being

7

somewhat disorganized in that area at the time it passed that triangle. A large active cold pool stretched from the front of the main squall line to the back edge of the stratiform precipitation in western Oklahoma.

From 0500 to 0700 UTC, a supercell at the south end of the squall line separated from the rest of the line. This separation is shown in the form of a gap in the front indicated by lower FSs and the lack of significant radar returns (Fig. 1c). The southern cell had weaker FSs than the more well defined squall line to the northeast. The region of strong divergence was primarily concentrated in northern Oklahoma, with a smaller area of strong divergence behind the southern supercell. Cold pools were identified in both of these areas. In western Oklahoma a few small convective cells had formed behind the secondary convergence line.

By 0900 UTC the southern supercell had progressed southeastward much farther away from the rest of the line while the main squall line continued eastward (Fig. 1d). The area of strong divergence behind the front was more concentrated on the southern half of the squall line. There was a weaker front to the east of the southern supercell. Behind the supercell to the northwest, trailing convection developed over the previous 2 hrs and eventually merges with the southern supercell (not pictured). There was clear separation between the convergence and divergence regions in the trailing convection. Overall, the front analysis performed well at representing the location of the front that would be expected based on the radar images. Despite the separation in the front, the cold pool along the front almost extended from the southern border with Texas to the northern border with Kansas. Notably, the cold pool extended back behind the front in eastern Oklahoma, suggesting a long-lived cold pool. At this time, the main cold pool has been in place for hours and has advanced eastward over time behind the squall line. However, large areas of stratiform precipitation were not classified as in a cold pool because the divergence values were not high enough at 0900 UTC. Many of the triangles in northeastern Oklahoma would likely be defined

8

as in a cold pool using a different definition relying more on sustained stratiform precipitation or lingering temperature falls.

*b. 15-16 June 2002 Case*

Around 1800 UTC 15 June, a line of thunderstorms oriented from northwest to southeast was located in northern Kansas and southern Nebraska moving southeastward. Over the next few hours the line merged with pop up thunderstorms in western Kansas and spread out allowing for a much more southwest to northeast oriented storm front to develop as the combined system moved south towards the Oklahoma border. The frontal passage and cold pool (Fig. 2) analysis for this event are shown.

At 0000 UTC 16 June the squall line had just entered the northwest corner of Oklahoma. Very strong convection was present ahead of the line, including triangles over 50 km ahead of the squall line (Fig. 2a). Divergence behind the front was present as well since this line had developed into a mature system several hours earlier. The FSs exceeded the strong front threshold. A few isolated triangles along and just behind the line were designated as cold pools at this time. Presumably, the cold pool extended into Kansas.

Ninety minutes later the squall line had progressed into the state reaching from almost the southwest corner to the northeast corner of Oklahoma (Fig. 2b). The stronger radar echoes were in the western half of the squall line, matching up with the stronger FSs. Additionally, the convergence-divergence pattern ahead of and behind the front was more well-defined in the western half of the state though present throughout the squall line. A broad region of heavy stratiform precipitation was located in northern Oklahoma. In that stratiform precipitation region a cold pool was detected far behind the squall line. Additionally, along the front there was a narrow band of scattered triangles that are in cold pool status, just behind strong convective cells.

9

By 0300 UTC the eastern half of the squall line had lost much of its strong convection resulting in a front that does not extend all the way to the Arkansas border (Fig. 2c), or at least not a front strong enough to meet the minimum threshold in this study. The southwestern corner of Oklahoma still featured strong convection, with the line extended towards north central Texas. The eastern half of the state had lost most of its divergence behind the line as the convective structure had fallen apart. However, there was still a narrow region of convergence ahead of the squall line. South central Oklahoma had a very large area of divergence behind the front. This extended up into north central Oklahoma with the trailing portion of the stratiform precipitation region. A small line of convergence was detected in the stratiform precipitation region in north central Oklahoma with an additional larger line of convergence behind the stratiform precipitation. There were many triangles experiencing a cold pool in south central Oklahoma behind the squall line. Extending back several triangles deep, this cold pool covered roughly one eighth of the state. The eastern half of the state had much less cold pool coverage in this analysis though a couple triangles in the northeast corner were still in a cold pool where the front had passed over an hour prior.

As the system moved farther southeast the strength of the convection in Oklahoma weakened further as the strongest cells to the west moved into Texas. The stratiform region of precipitation was well-defined and contained a large area of divergence behind the remnants of the squall line in Oklahoma (Fig. 2d). The line of convergence that was just behind the stratiform precipitation region had fallen farther behind the precipitation though it maintains an almost continuous line through a large portion of the northwest to north central region. The cold pool was concentrated in the south central stratiform precipitation with a few solitary triangles elsewhere in cold pools.

10

*c. 20 May 2011 Case*

One of the more notable cases during the Mid-Latitude Continental Convective Clouds Experiment (MC3E) occurred on 20 May 2011 (Fig. 3). Scattered convective cells formed in central Oklahoma and by 0400 UTC the cells stretched from the Oklahoma-Texas border southwest to the Texas panhandle. These cells organized into a squall line and started to build northward through southwestern Oklahoma with the fronts and cold pools tracked with the algorithm.

At 0900 UTC (Fig. 3a) the front analysis showed a strong front stretching from southwestern Oklahoma northward. There was a well-defined squall line as well as convergence ahead of the front with areas of strong divergence behind the front. The structure of the line appeared less organized at the northern end of the front as strong convection juts out ahead of the rest of the front. This was due to an isolated thunderstorm from earlier that was merging into the squall line. Due to the merging of that thunderstorm, the frontal boundary was not as well defined in that area and there was only some semblance of a convergence-divergence couplet. Since the line had just developed northward into the area the previous two hrs, only two triangles had cold pools present at 0900 UTC.

Over the next couple of hours the squall line builds throughout northern Oklahoma. By 1100 UTC the line had developed a bow shape (Fig. 3b). Notably, the easternmost part of the bow had lower FSs and contained a break in the high convergence area as well as having slightly lower radar returns. However, a strong divergence area behind the line did remain intact in that region. The northern part of the squall line had convergence ahead of the front but the FSs at some stations were not high enough to trigger a front to be drawn in that area. Since the northern edge of the front was the most recent to form, it was not strong enough to meet minimum front score thresholds. A distinct line of triangles containing cold pools stretched through two thirds of the meridional

11

length of the state just behind the front. Unlike the 1997 case, the cold pool did not extend as far back behind the front.

From 1100 to 1300 UTC the northern part of the bow began to fall apart. Convection ahead of the front led to a more scattered area of thunderstorms in northeastern Oklahoma (Fig. 3c) as well as thunderstorms popping up several counties east of the squall line. The structure of the line was oriented southwest to northeast by 1300 UTC. The front analysis retained the southern half of the front as meeting the strong front threshold while a few triangles on the northern end had the lower FS threshold met. Similarly, the cold pool area had decreased with only the southern Oklahoma portion of the front managing to exceed the divergence threshold.

The front continued through the state, exiting through northeastern Oklahoma around 1500 UTC (Fig. 3d) while the southern end of the front exited the state a couple hrs later before a second line of storms moves into southeastern Oklahoma. There were no areas of strong divergence behind the northeastern Oklahoma portion of the front. The cold pool region covered only a few triangles in southeastern Oklahoma.

*d. 24-25 May 2011 Case*

The final case study is another system that occurred during the MC3E experiment a few days after the previous case. On 24 May the 1800 UTC sounding (not shown, UCAR archive) from Norman, Oklahoma (KOUN) had strong southerly winds at low-levels veering with height. A strong stable layer at roughly 825 mb was in place; however, low-level moisture and unstable mid-levels resulted in CAPE values over 2500 $Jkg^{-1}$. The Storm Prediction Center (SPC) had issued a high risk convective outlook for central and northeastern Oklahoma.

By 2000 UTC the first thunderstorm cells had formed, rapidly developing into severe thunderstorms with a threat of tornadoes. The frontal passage and cold pool (Fig. 4) analysis had some

difficulty capturing the front and any associated cold pool with these thunderstorms due to the low resolution of the Mesonet station grid (Fig. 4a). There was a large region of convergence both ahead of and behind the supercells at this time. The front, although strong, did not extend throughout all of the supercells, and only one triangle observed a cold pool at this time.

Over the next couple hrs, more cells had flared up and a clear north-south line had formed (Fig. 4b) though there were gaps between the cells that made up the line. There was only a slight signature of the usual convergence-divergence pattern ahead of and behind the front, likely, though not necessarily, a result of the strong rotation in tornadoes, or systems capable of potentially producing tornadoes. At this point multiple tornadoes had formed, including one that struck the El Reno Mesonet station at 2120 UTC recording a maximum wind gust of 151 mph. Only a few stations in north central and northwestern Oklahoma observed cold pools at the time. Strong rotation tends to lead to surface inflow from all directions, reducing the likelihood of divergence and cold pools behind a front in this situation.

By 0000 UTC, however, the squall line was straighter and had fewer, smaller gaps between individual storm cells (Fig. 4c). A convergence-divergence distribution ahead of and behind the front was more well-defined in the north central Oklahoma line and the smaller, weaker (in terms of front strength) line in south central Oklahoma. A large region of convergence is present in western Oklahoma where a secondary front was present that lacked precipitation. Cold pool coverage had grown behind the main line in central Oklahoma. Additionally, one triangle was marked as in a cold pool in the northwest corner of Oklahoma. Generally, the lack of stratiform precipitation makes it likely that this case is closer to what other studies would identify in terms of cold pool area compared to the other cases in this chapter.

As the main front progressed further eastward the strength of the front weakened slightly with regards to FSs (Fig. 4d). However, convection was still intense with radar echoes reaching up to

13

60 dBZ. The fronts in western Oklahoma had a disorganized structure and covered more area at this time. The cold pools at 0200 UTC remained just behind the main front with one triangle in western Oklahoma in a cold pool as well. Radar coverage in northwestern Oklahoma was sparse by comparison, though the secondary line does not appear to develop precipitation as it moves throughout the state the next few hours. At 0300 UTC (not shown) there was a faint green line visible on the radar signifying this secondary front.

*e. Cold Pool Time Series*

Observing the change in cold pool area over time allows for greater visualization of the size and time scales of the areas experiencing a cold pool (Fig. 5).

From roughly 0300 to 1100 UTC in the 13 June 1997 case at least one Mesonet triangle resided in a cold pool (Fig. 5a). The peak size of cold pool area was around 0930 UTC at a size of nearly $1.4 \times 10^{10}$ m$^2$. Around a third of the cold pool areas retained a cold pool for at least 30 mins, and some triangles, particularly later in the period, retained cold pool status for over an hr.

For the 15-16 June 2002 case the cold pool time series shows a larger maximum cold pool area than the first case study with a maximum size of roughly $1.8 \times 10^{10}$ m$^2$ (Fig. 5b). The duration of the cold pools tended to be longer than the first case study. Later in the time period over half the cold pool area comprised of locations which had been in a cold pool for half an hr or more. The cold pool area that was present for at least an hr peaked at roughly $5 \times 10^9$ m$^2$ around 0400 UTC.

For the 20 May 2011 case the cold pool time series showed a longer lasting period from initial to final cold pool and a lower maximum cold pool area that only reached roughly $8 \times 10^9$ m$^2$ (Fig. 5c). There are frequent jumps in the amount of area covered by cold pools. Many of the cold pools lasted half an hr; however, very few triangles maintained a cold pool for at least an hr.

14

Considering the narrow width of the divergence region behind the storm line and the speed of the front, this result was expected.

The cold pool time series for the final case study showed a maximum cold pool area of just over $1.1 \times 10^{10}$ m$^2$ (Fig. 5d). The entire period with cold pools present lasted approximately 10 hrs. The cold pools were rather short in duration with few lasting even half an hr. Cold pools later in the event had longer durations than cold pools in the first half of the event, a result likely due to the increased organization of the convergence-divergence gradient across the front over time.

*f. Front Characteristics*

For each of the four case studies the average divergence, temperature, and pressure timeseries were identified and centered on the time step when the front was halfway through the Mesonet triangle. For temperature and pressure each triangle uses the average of the three corner Mesonet stations. The average time series is plotted along with the standard deviation for each variable and case (Fig. 6). For temperature and pressure, the values are normalized to 0 at the midpoint of frontal passage. As a result, the standard deviation near the midpoint was artificially low so the standard deviations for temperature and pressure 15 minutes before and after the frontal passage midpoint are removed. The x-axis was reversed on the plot to show a west to east pattern.

For all four cases, the divergence profile begins in similar fashion with a dip towards strong convergence values before a reversal to strong divergence as the front crosses the triangle. However, for three of the cases the average divergence trends back towards 0 after the frontal passage while for the 15-16 June 2002 case the average divergence remains at an elevated level even two hours after the middle of frontal passage.

Temperature profiles start similarly with temperatures around 3-4 K higher on average before frontal passage than in the middle of a frontal passage. The drop in temperature begins around 30-

15

45 minutes before the middle of a frontal passage and continues until around 15 minutes afterwards generally. After frontal passage three of the cases show a slight rebound in temperature of 1-2 K. On the other hand, the temperature continues to decrease on average for the 20 May 2011 case.

Pressure profiles start with a wide range of lower pressure values before frontal passage but show an increasing trend during frontal passage. For the 13 June 1997 and 15-16 June 2002 cases there is a drop off in pressure after frontal passage, while for the 24-25 May 2011 case the average pressure drop after frontal passage is minimal. For the 20 May 2011 case the pressure continues to slightly increase.

*g. Front Wind Maps*

Using the front locations from the case studies plots of front propagation speed can be made for the case studies (Fig. 7) and (Fig. 8). These plots help identify characteristics of the front such as the separation in the 13 June 1997 case where the main storm line propagates to the east southeast while the southern supercell moves more southward at a slower speed (Fig. 7a). Propagation speeds are roughly a factor of 2 different in that instance. Generally, front speeds are similar in adjacent triangles with the five minute time resolution being a contributor to the differences.

The 15-16 June 2002 case shows near uniform south to southeast flow through Oklahoma with wind speeds primarily around 20 ms$^{-1}$ (Fig. 7b). An exception is around 0400 UTC when most triangles experiencing a front are closer to 10-15 ms$^{-1}$. Around this time the primary area of strong convection was in southwestern Oklahoma which ended up surging farther ahead of the stratiform precipitation regions to the east where the front speed appears to slow.

The storm line in the 20 May 2011 case developed from southwestern Oklahoma and northern Texas with storms moving towards the northeast as the line propagates eastward (Fig. 8a). With the line building towards the north, the northern Oklahoma quivers have more of a northward

16

component. Elsewhere in the state the southwest-northeast oriented line moves eastward so the storm line itself sweeps through in an east-southeasterly direction. The front moves faster in north-central Oklahoma triangles due to the advancing storm cells moving towards the north. The slower speeds in eastern Oklahoma are due to the slower propagation of the line compared to the faster propagation of individual storm cells along the line.

In the 24-25 May 2011 case the front speed is generally 10-15 ms$^{-1}$ across Oklahoma (Fig. 8b). The front itself propagates east-southeastward though the storm cells that make up the line move from the southwest to northeast.

## 4. Conclusions

The four cases studies analyzed represent a very small fraction of the 15 yrs of Mesonet data. However, they highlight varying storm structures and profiles of key variables.

The 13 June 1997, 15-16 June 2002, and 20 May 2011 cases involve MCSs tracking through the Mesonet with a strong forward line of thunderstorms with a large region of trailing stratiform precipitation. In contrast, the 24-25 May 2011 case involved supercells which formed into a line crossing Oklahoma, with more rotation which likely resulted in the delayed formation of a convergence-divergence couplet in the storm line.

The cold pools in this study were similar to other studies in terms of length along a front. However, the width a cold pool extended behind the lead storm axis was typically only 50-100km in these cases while in other studies the distances can be 100-400 km for MCSs (Stensrud et al. 1999). Most triangles in the Mesonet case studies remained in cold pools for 30-60 mins while in other studies mean lifetimes can exceed 2 hrs (Tompkins 2001; Young et al. 1995).

Divergence, temperature, and pressure values were observed to have fairly similar case to case results though there were some exceptions. Strong convergence ahead of the front was followed by

17

a rapid transition to strong divergence immediately behind a front. Temperatures dropped around 3-6 K on average with the frontal passage in the four cases while pressure increased 1-4 mb on average in 3 of the 4 cases.

This study utilized 15 yrs of Oklahoma Mesonet surface observations to identify over ten thousand of Mesonet triangle fronts and cold pools. These four cases detailed here cover a couple hundred of them while Part I looked at climatological statistics. The data here is at roughly 40 km resolution, which can be useful when many general circulation models use similar or slightly higher resolution.

# References

Anber, U., S. Wang, and A. Sobel, 2014: Response of atmospheric convection to vertical wind shear: Cloud-system-resolving simulations with parameterized large-scale circulation. Part I: Specified radiative cooling. *J. Atmos. Sci.*, **71**, 2976–2993.

Brock, F. V., K. C. Crawford, R. L. Elliott, G. W. Cuperus, S. J. Stadler, H. L. Johnson, and M. D. Eilts, 1995: The Oklahoma Mesonet: A technical overview. *J. Atmos. Oceanic. Technol.*, **12**, 5–19.

Cheng, M.-D., and A. Arakawa, 1997: Inclusion of rainwater budget and convective downdrafts in the Arakawa-Schubert cumulus parameterization. *J. Atmos. Sci.*, **54**, 1359–1378.

Coleman, T. A., and K. R. Knupp, 2009: Factors affecting surface wind speeds in gravity waves and wake lows. *Wea. Forecasting*, **24**, 1664–1679.

Coleman, T. A., and K. R. Knupp, 2011: A review of three significant wake lows over Alabama and Georgia. *Wea. Forecasting*, **26**, 766–773.

Dione, C., M. Lothon, D. Badiane, B. Campistron, F. Couvreux, F. Guichard, and S. M. Sall, 2014: Phenomenology of Sahelian convection observed in Niamey during the early monsoon. *Quart. J. Roy. Meteor. Soc.*, **140**, 500–516.

Droegemeier, K. K., and R. B. Wilhelmson, 1985: Three-dimensional numerical modeling of convection produced by interacting thunderstorm outflows. Part I: Control simulation and low-level moisture variations. *J. Atmos. Sci.*, **42**, 2381–2403.

Fujita, T. T., 1955: Results of detailed synoptic studies of squall lines. *Tellus*, **7**, 405–436.

Fujita, T. T., and R. M. Wakimoto, 1980: Five scales of airflow associated with a series of down-bursts on 16 July 1980. *Mon. Wea. Rev.*, **109**, 1438–1456.

Johnson, R. H., 1976: The role of convective-scale precipitation downdrafts in cumulus and synoptic-scale interactions. *J. Atmos. Sci.*, **33**, 1890–1910.

Johnson, R. H., and M. E. Nicholls, 1982: A composite analysis of the boundary layer accompanying a tropical squall line. *Mon. Wea. Rev.*, **111**, 308–319.

Kain, J. S., and J. M. Fritsch, 1990: A one-dimensional entraining/detraining plume model and its application in convective parameterization. *J. Atmos. Sci.*, **47**, 2784–2802.

Lesage, A. T., and S. K. Krueger, 2016: Fronts and convective cold pools in the Oklahoma Mesonet. Part I: 15-year climatology. *Mon. Wea. Rev.*, submitted.

Li, Z., P. Zuidema, and P. Zhu, 2014: Simulated convective invigoration processes at trade-wind cumulus cold pool boundaries. *J. Atmos. Sci.*, **71**, 2823–2841.

Mapes, B. E., and R. Neale, 2011: Parameterizing convective organization to escape the entrainment dilemma. *J. Adv. Model. Earth Syst.*, **3**, M06 004.

McPherson, R. A., and Coauthors, 2007: Statewide monitoring of the mesoscale environment: A technical update on the Oklahoma Mesonet. *J. Atmos. Oceanic Technol.*, **24**, 301–321.

Moorthi, S., and M. J. Suarez, 1991: Relaxed Arakawa-Schubert: A parameterization of moist convection for general circulation models. *Mon. Wea. Rev.*, **120**, 978–1002.

Nicholls, M. E., and R. H. Johnson, 1984: A model of a tropical squall line boundary layer wake. *J. Atmos. Sci.*, **41**, 2774–2792.

Pan, D.-M., and D. A. Randall, 1998: A cumulus parameterization with a prognostic closure. *Quart. J. Roy. Meteor. Soc.*, **124**, 949–981.

Qian, Y., G. S. Young, and W. M. Frank, 1998: A convective wake parameterization scheme for use in general circulation models. *Mon. Wea. Rev.*, **126**, 456–469.

Rotunno, R., J. B. Klemp, and M. L. Weisman, 1988: A theory for strong, long-lived squall lines. *J. Atmos. Sci.*, **45**, 463–485.

Rozbicki, J. J., G. S. Young, and Y. Qian, 1999: Test of a convective wake parameterization in the single-column version of CCM3. *Mon. Wea. Rev.*, **127**, 1347–1361.

Stensrud, D. J., G. S. Manikin, E. Rogers, and K. E. Mitchell, 1999: Importance of cold pools to NCEP mesoscale Eta model forecasts. *Wea. Forecasting*, **14**, 650–670.

Tompkins, A. M., 2001: Organization of tropical convection in low vertical wind shears: The role of cold pools. *J. Atmos. Sci.*, **58**, 1650–1672.

Wakimoto, R. M., 1982: The life cycle of thunderstorm gust fronts as viewed with Doppler radar and rawinsonde data. *Mon. Wea. Rev.*, **110**, 1060–1082.

Young, G. S., S. M. Perugini, and C. W. Fairall, 1995: Convective wakes in the equatorial western Pacific during TOGA. *Mon. Wea. Rev.*, **123**, 110–123.

Zipser, E. J., 1977: Mesoscale and convective-scale downdrafts as distinct components of squall-line structures. *Mon. Wea. Rev.*, **105**, 1568–1589.

Zuidema, P., and Coauthors, 2012: On trade wind cumulus cold pools. *J. Atmos. Sci.*, **69**, 258–280.
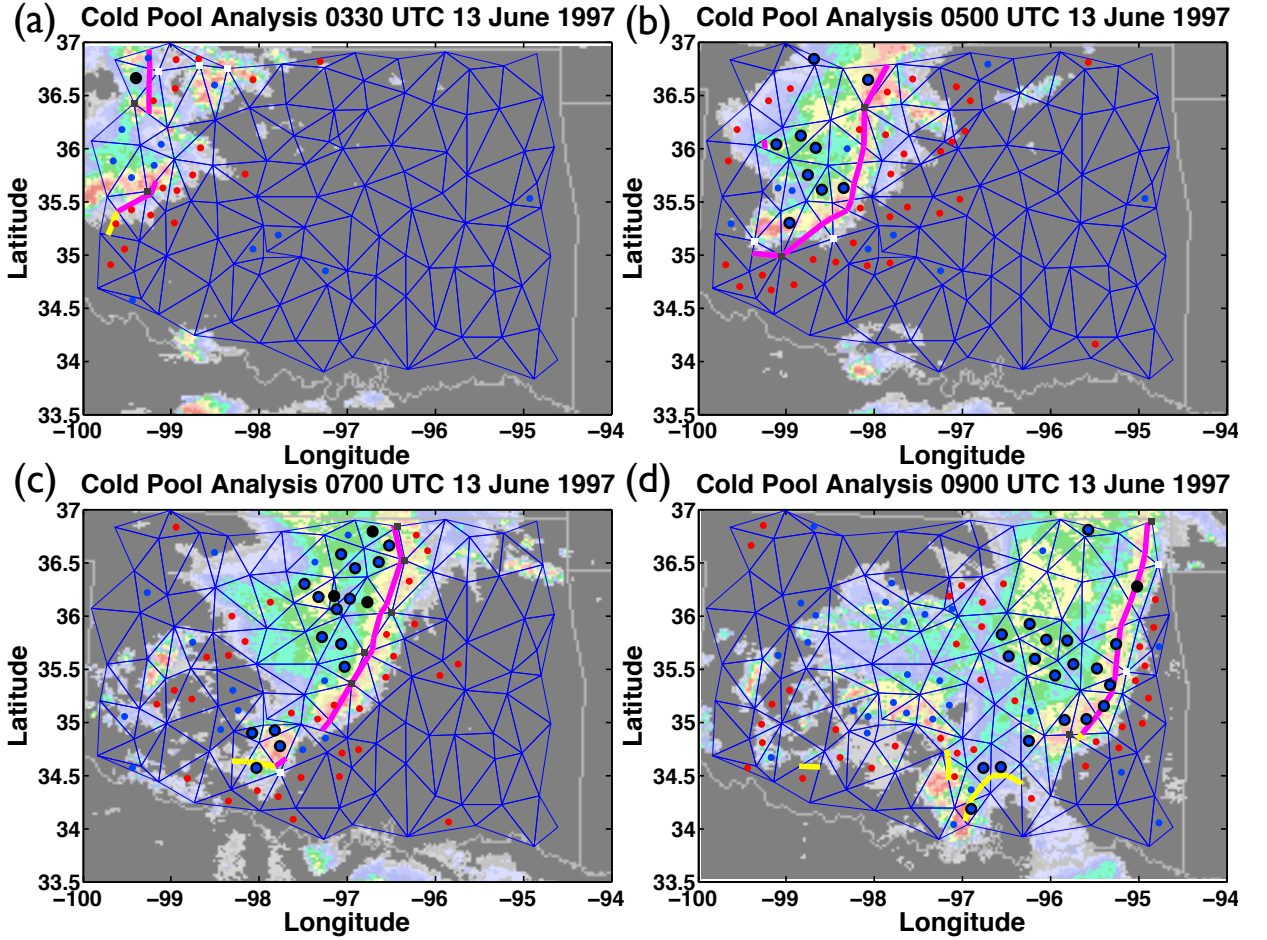
# LIST OF FIGURES

FIG. 1. Front and cold pool analysis for 13 June 1997 (a) 0330 UTC, (b) 0500 UTC, (c) 0700 UTC, and (d) 0900 UTC. Red dots are $D_i < -10^{-4}\text{s}^{-1}$ while blue dots are $D_i > 10^{-4}\text{s}^{-1}$. Yellow lines are frontal passages with FSs of $3 <= \text{FS} < 5$ while magenta lines are frontal passages with FSs of 5+. White squares are stations where at the current timestep the FS is $3 <= \text{FS} < 5$; gray squares designate stations currently with FSs at 5+. Black dots indicate triangles currently designated as cold pools. Radar images are from the UCAR image archive, NEXLAB - College of DuPage.

FIG. 2. Same as Figure 1 except for 16 June 2002 (a) 0000 UTC, (b) 0130 UTC, (c) 0300 UTC, and (d) 0430 UTC.
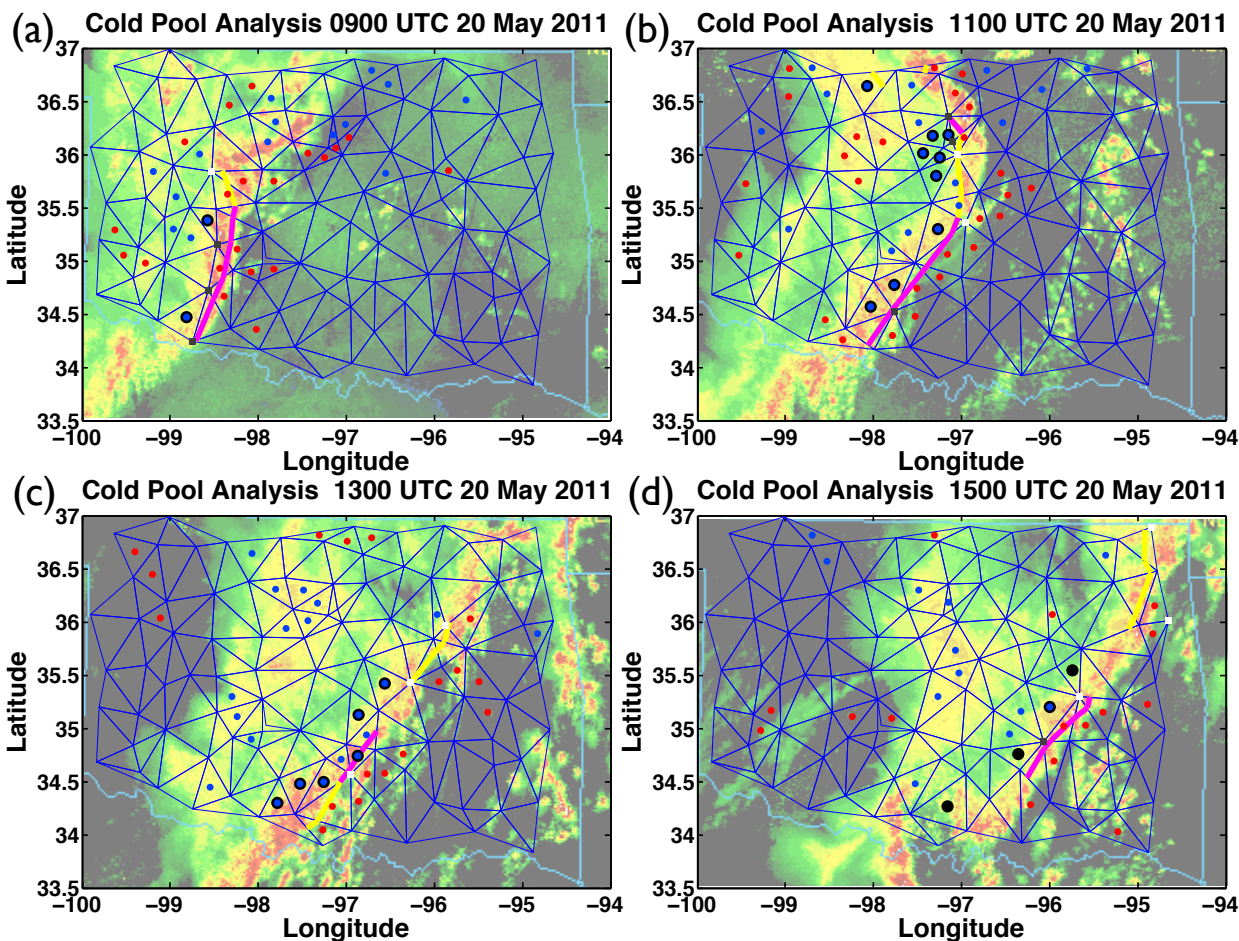
24

FIG. 3. Same as Figure 1 except for 20 May 2011 (a) 0900 UTC, (b) 1100 UTC, (c) 1300 UTC, and (d) 1500 UTC.
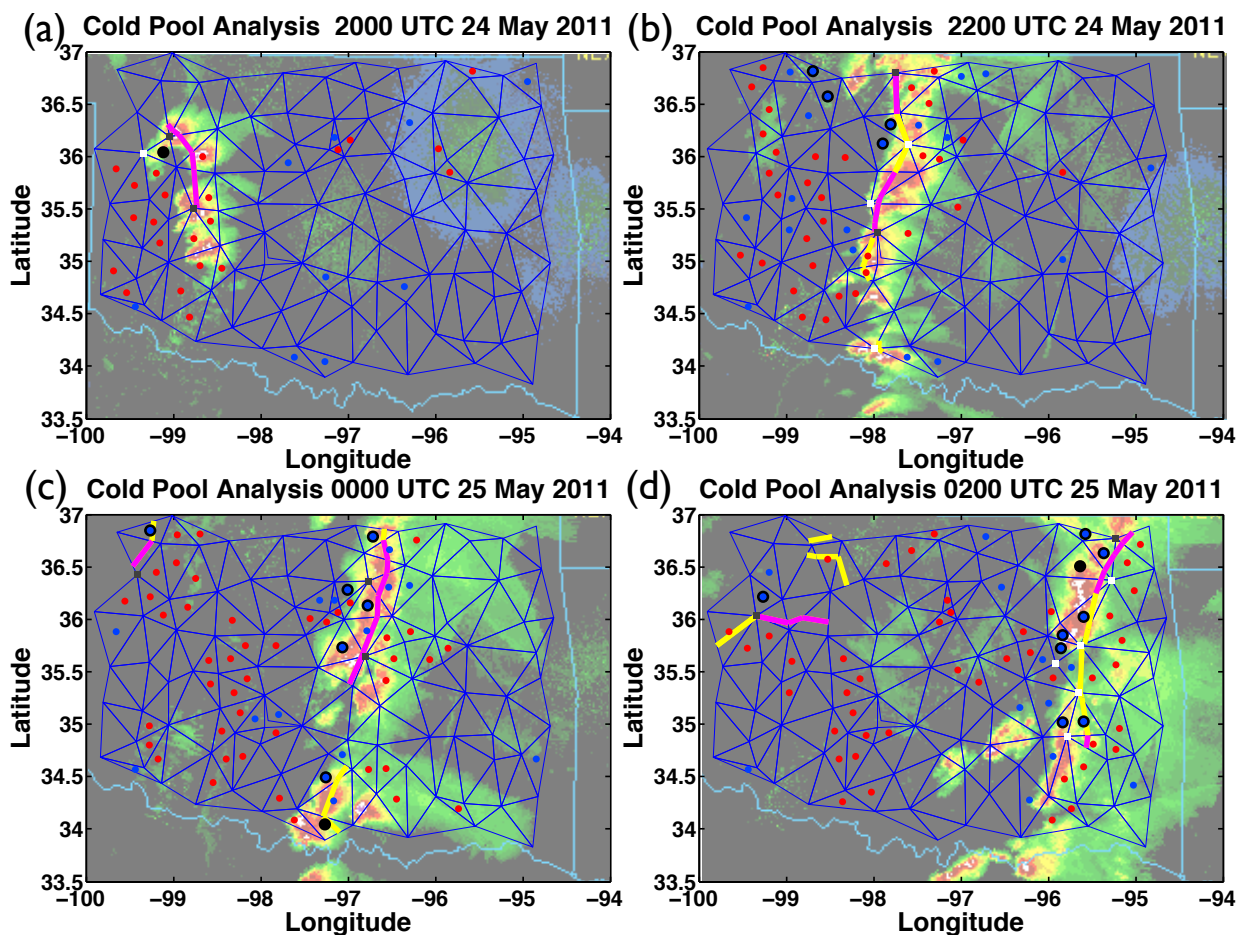
FIG. 4. Same as Figure 1 except for 24 May 2011 (a) 2000 UTC, (b) 2200 UTC, 25 May 2011 (c) 0000 UTC, and (d) 0200 UTC.
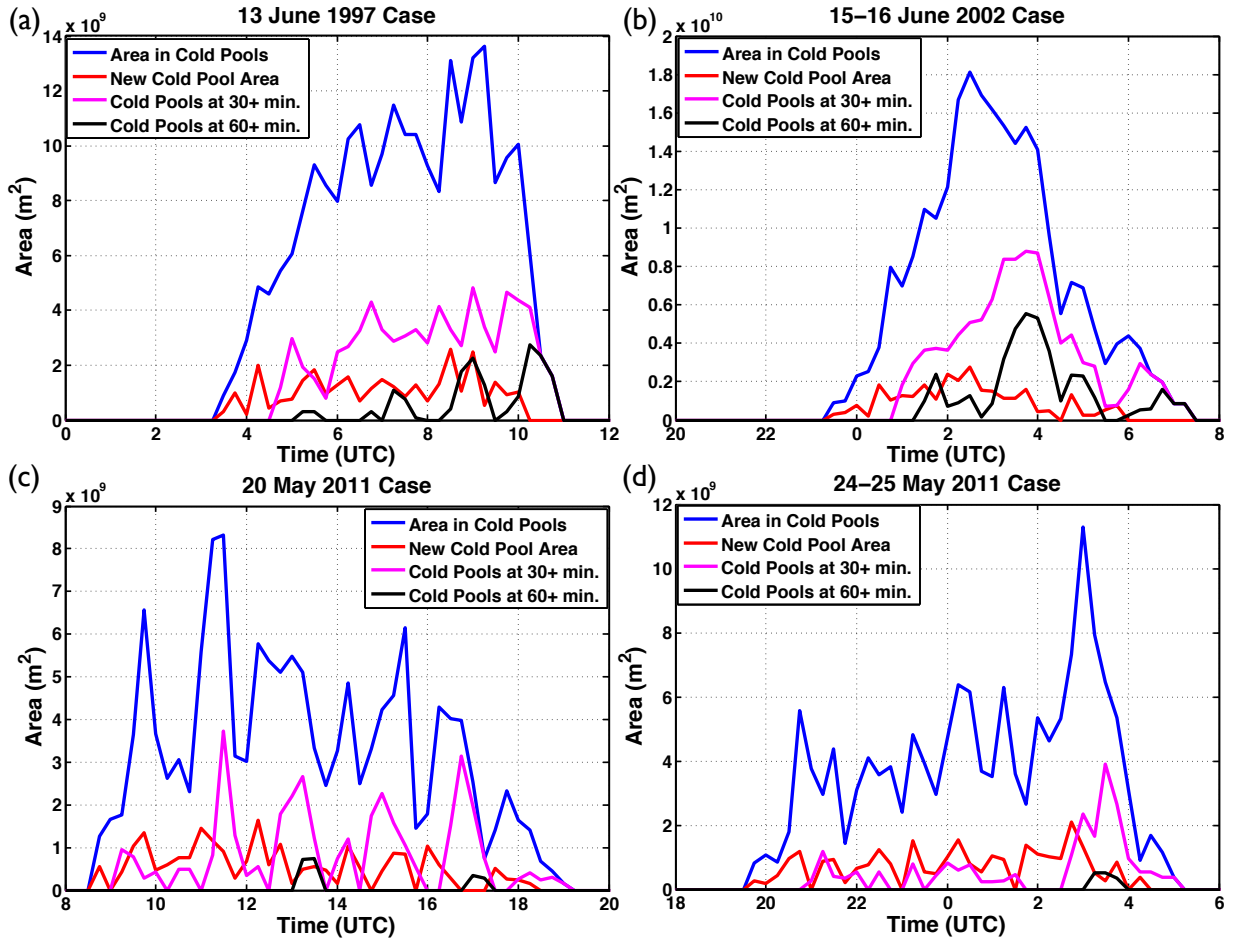
FIG. 5. Cold pool areas for the case studies: a) 13 June 1997 0-12 UTC, b) 15-16 June 2002 20-8 UTC, c) 20 May 2011 8-20 UTC, d) 24-25 May 2011 18-6 UTC. Cold pool areas are shown as 15 minute averages for total area in cold pools (blue), new cold pool area (red), area residing in a cold pool at least 30 mins (magenta), and area residing in a cold pool at least 60 mins (black).
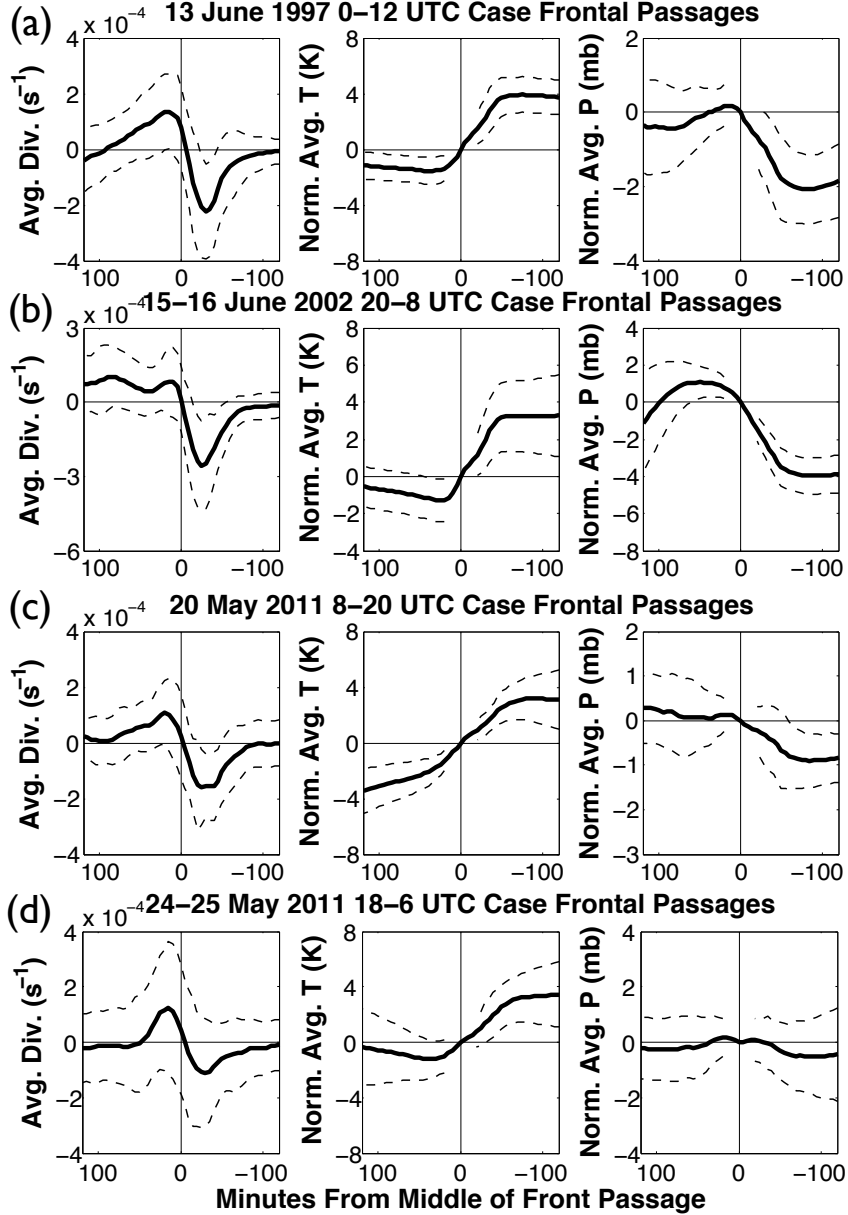
FIG. 6. Average (solid) and +- 1 standard deviation (dashed) divergence, normalized temperature, and normalized pressure values for frontal passages at Mesonet triangles. The x-axis is reversed to show a west to east pattern. Case studies are: a) 13 June 1997 0-12 UTC, b) 15-16 June 2002 20-8 UTC, c) 20 May 2011 8-20 UTC, d) 24-25 May 2011 18-6 UTC.
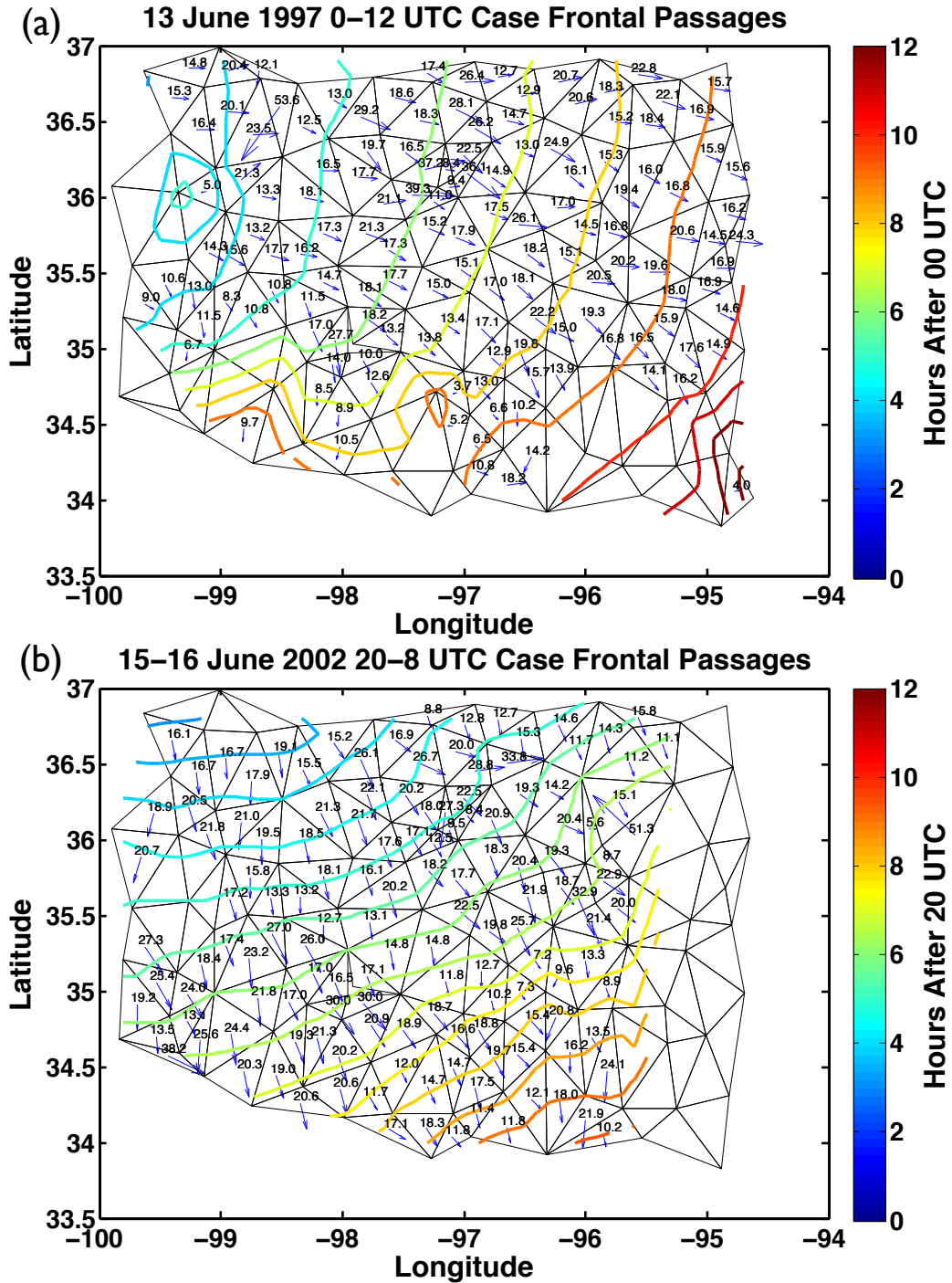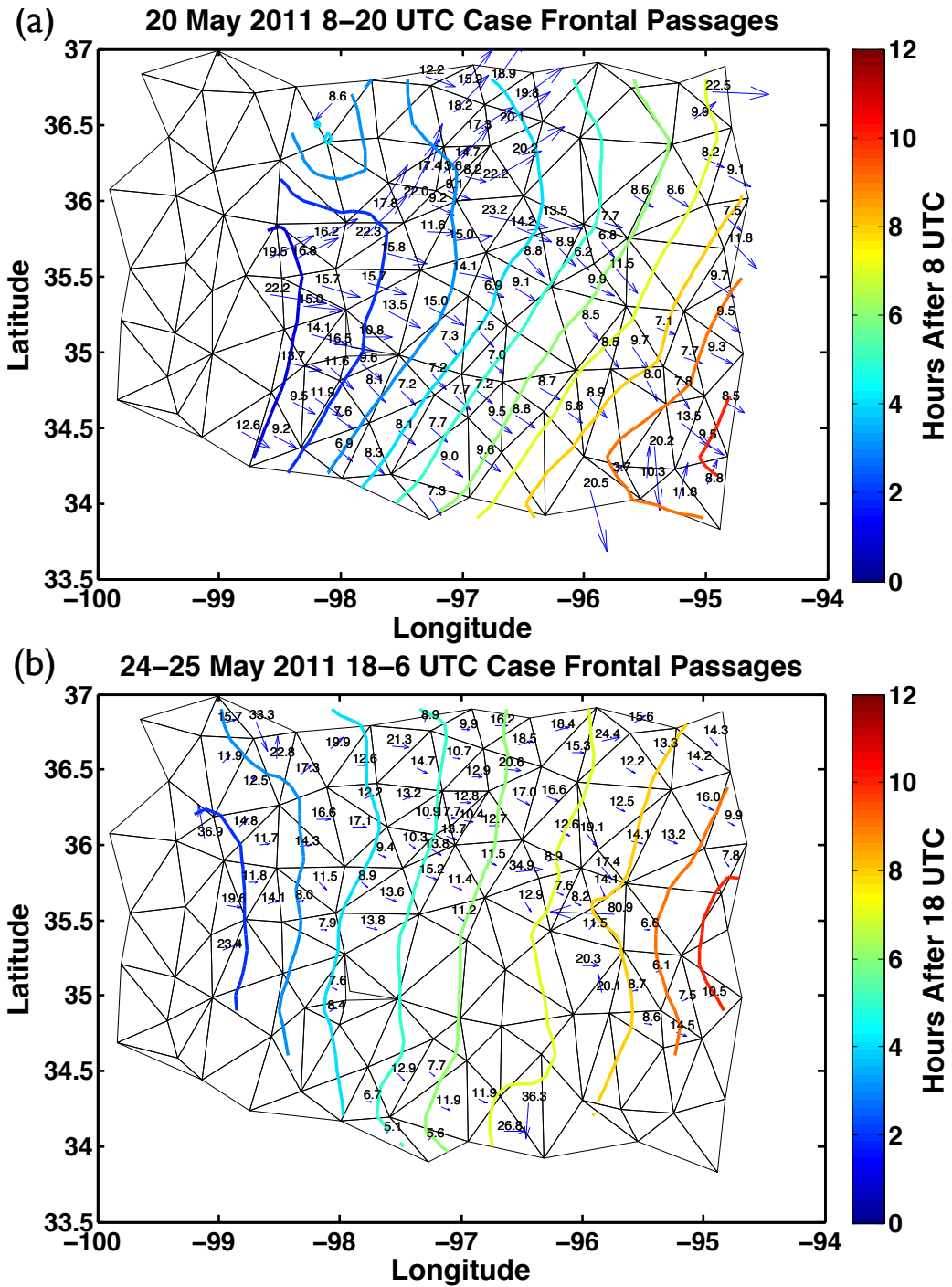
FIG. 7. Frontal passage location and timing (contours) with front speeds (in m s$^{-1}$) represented by quivers. Case studies are: a) 13 June 1997 0-12 UTC and b) 15-16 June 2002 20-8 UTC.

FIG. 8. Frontal passage location and timing (contours) with front speeds (in m s$^{-1}$) represented by quivers. Case studies are: a) 20 May 2011 8-20 UTC and b) 24-25 May 2011 18-6 UTC.